An Inductive Power Transfer Converter with Irradiance-Adaptive Hybrid MPPT Control Strategy for Floating-PV System

Chio-Kuan Choi, Io-Wa Iam, Iok-U Hoi, Chi-Seng Lam
State Key Laboratory of Analog and Mixed-Signal VLSI, University of Macau, Macao, China
Institute of Microelectronics, University of Macau, Macao, China
Department of Electrical and Computer Engineering, Faculty of Science and Technology, University of Macau, Macao, China
E-mail: cslam@um.edu.mo, C.S.Lam@ieee.org

IECON 2021 - 47th Annual Conference of the IEEE Industrial Electronics Society | 978-1-6654-3554-3/21/$31.00 ©2021 IEEE | DOI: 10.1109/IECON48115.2021.9589492

***Abstract*—The market share of renewable energy grows rapidly with the rising issues like global warming and environment pollution. As a kind of flexible and mature way to collect solar energy, photovoltaic (PV) panels have been widely installed on lands. To save precious land resources, PV panels can be installed on water to form floating-PV farm. In this paper, an inductive power transfer (IPT) converter for wireless power transmission is proposed for the floating-PV system, which can avoid of possible electrical hazard and reduce the exposure of the components, thus enhance the performance of anti-humidity and anti-salinity of the floating-PV system. However, the varying irradiance conditions caused by changeable weather of lake or seashore scenario gives challenge to the trackable range of MPPT control strategy for the IPT converter. To address this problem, an irradiance-adaptive hybrid maximum power point tracking (MPPT) control strategy for the floating-PV system is also proposed, which can achieve the maximum power point (MPP) of the PV panels even under a wide range of irradiance conditions. In addition, the IPT converter with the proposed MPPT control strategy does not require a DC-DC converter to achieve the MPPT in a wide irradiance range, thus saving the system cost. Finally, the IPT converter with irradiance-adaptive hybrid MPPT control strategy is theoretically analyzed, and its feasibility is verified on an experiment platform.**

***Index Terms*—Inductive power transfer, floating-PV, photovoltaic, irradiance-adaptive hybrid maximum power point tracking (MPPT)**

I. Introduction

With the growing concerns of global warming and environment pollution, renewable energy starts to play an important role in global energy market. According to [1], the weight of renewable energy in global mix grew with a steady speed and occupied a share of 26.2% by 2018, of which solar power plants provided 2.4% of the world electricity generation. Also, 65.4% of the global investment in new power capacities went into renewables (excluding hydropower) in 2018 [1], which reveals the demand and market of renewable energy is enormous. As solar energy has many advantages comparing to other renewable energy like flexibility of location selection, scalability, fast infrastructure building speed and relatively low cost of infrastructure construction, solar energy is considered as a promising option for implementing renewable energy in a large scale.

Traditionally, photovoltaic (PV) power plants were chosen to build on land or the roof of the buildings. But with the considerations of scarcity of land and other issues like large PV power plants could cause significant heat islanding effect in cities [2], people started to pay more attention on floating-PV system. Floating-PV system is a kind of solution that mounting PV panels on floating blocks to form a PV panel array on a lake or a sea, and it has been proved to be advantageous for multiple aspects as follows. In terms of energy production, due to a lower environment temperature comparing to the case installed on land, the efficiency of PV panels can be higher and can yield larger output power. Also, from the perspective of environment, floating-PV system saves limited land resource, and can control algal bloom and water evaporation by blocking exceed sunlight [2].

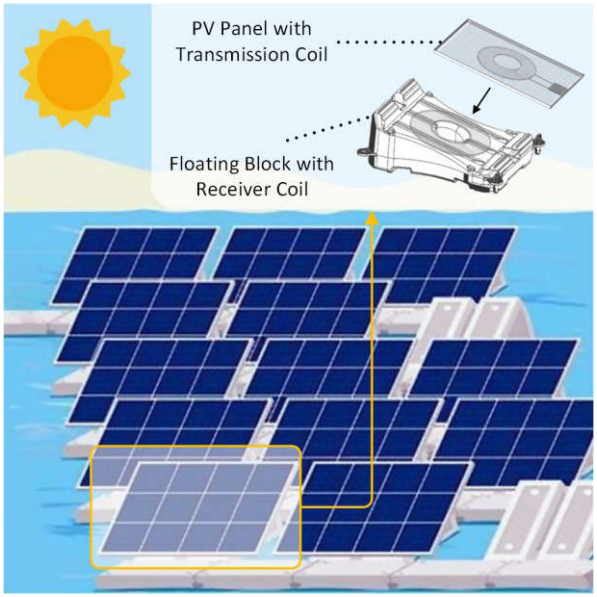

Fig. 1. Schematic of wireless power transfer used in floating-PV system.

However, lacustrine and marine environments are usually with characteristics of high humidity and high salinity. Based on the research in [3], the most damaging climates for the PV panel is the warm and humid environment, and [4] also shows that high salinity environment could cause PV panel failures like degradation of the polymer and corrosion of the metallic components. Therefore, the durability and maintainability of the floating-PV facilities should be taken careful consideration during construction. In this paper, an inductive power transfer (IPT) is used as the interface for the power transmission between PV panel and LVDC bus as shown in Fig. 1. The wireless power transmission scheme can greatly eliminate the connectors used in system, which can avoid of possible electrical hazard and reduce the exposure of the components,

This work was funded by The Science and Technology Development Fund, Macau SAR (FDCT) (File no. 0028/2020/A1, 025/2017/A1, and SKL-AMSV(UM)-2020-2022) and by the University of Macau (File no. MYRG2017-00090-AMSV). (Corresponding author: *Chi-Seng Lam*)

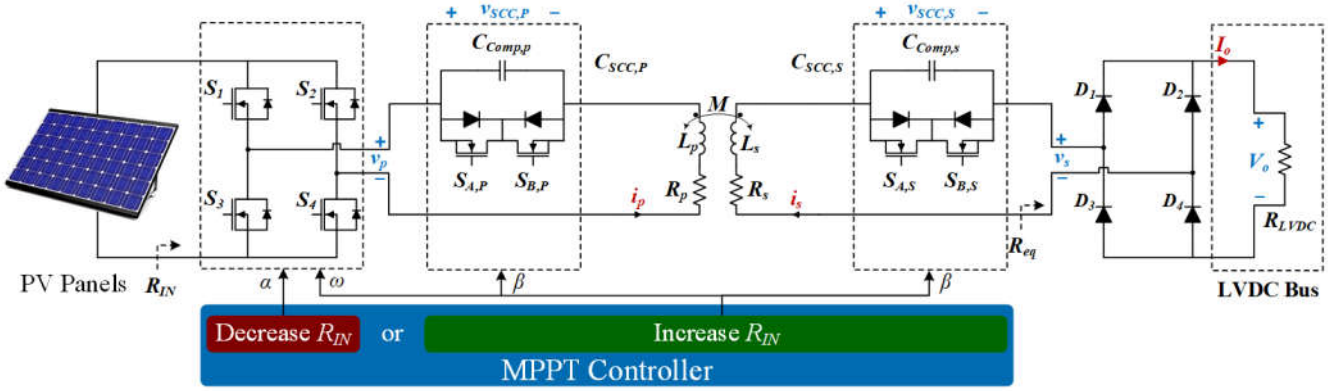

Fig. 2. System structure of the IPT converter with proposed MPPT control strategy.

thus enhance the performance of anti-humidity and anti-salinity of the floating-PV system. In addition, facing the problem of cracks or degradation of the PV panel, the replacement of the panel only requires simple mounting without reconnecting cables, which also simplifies the maintenance process.

With regard to a PV power plant, because of the inherent characteristics of the PV panel and the variation of environmental factors like irradiance, temperature, etc., the maximum power point tracking (MPPT) is usually required to allow the system to generate maximum power under any circumstances. For a PV array consist of several PV panels, the irradiance conditions can be classified as uniform and non-uniform. Uniform irradiance means all PV panels in a PV array have the same irradiance condition and the P-V curve of the system has a global maximum power point (GMPP). Non-uniform irradiance means the irradiance condition of some PV panels in the array are different from the others, which can result in several local maximum points (LMPPs) in the P-V curve and only one of them is the GMPP. The uniform irradiance condition and non-uniform irradiance condition may alternately appears, especially under the changeable weather conditions in lake or seashore scenarios. Also, GMPP of these two conditions could be far apart, which gives a challenge to the trackable range of the MPPT control strategy. Therefore, an MPPT control strategy with wide tracking range is more needed comparing to the PV plant on land.

In general, the conventional wired PV system implements the MPPT by using an extra DC-DC converter [5]. Also, some research works like [6] and [7] applied a DC-DC converter to achieve MPPT for the wireless PV system. To reduce the complexity and cost of the overall system, this paper proposes an IPT system with hybrid MPPT control strategy for the floating-PV system that can achieve MPPT without using an additional DC-DC converter. The hybrid MPPT control is done by varying the operating frequency of the transmitter-side inverter, together with the switch-controlled compensation capacitor (SCC) to dynamically maintain zero phase angle of the IPT converter and track the MPP, or work at a fixed frequency and track the MPP by the phase shift (PS) modulation of transmitter-side inverter. This hybrid control strategy can work in a wide range and track MPP in both uniform and non-uniform irradiance cases.

The rest of this paper is arranged as follows. Section II describes the SS-IPT converter structure with its operating waveform diagram and analyzes its equivalent circuit model. In Section III, the proposed hybrid MPPT control strategy, including operating frequency modulation with capacitor compensation tracking and phase modulation, is analyzed. In Section IV, the experiment platform is built for the experimental verification. Finally, Section V concludes this paper.

II. System Modeling

A. System Structure

As shown in Fig. 2, the proposed wireless floating-PV system with hybrid MPPT control strategy includes PV panels, a series-series compensated IPT (SS-IPT) converter with switch-controlled compensation capacitor (SCC), and the output is connected to a LVDC bus.

The SS-IPT converter consists of a full bridge inverter formed by four MOSFET switches S_1 to S_4 at the PV transmitter-side. Conventional compensation capacitor is replaced by an SCC at both the PV transmitter-side and the receiver-side. The SCC at the PV transmitter-side includes MOSFET switches $S_{A,P}$ and $S_{B,P}$ and compensation capacitor $C_{comp,p}$. The SCC at the receiver-side includes MOSFET switches $S_{A,S}$ and $S_{B,S}$ and compensation capacitor $C_{comp,s}$. The SCCs can be regarded capacitor $C_{SCC,P}$ and $C_{SCC,S}$. The voltage across the SCC at both sides are v_{SCCP} and v_{SCCS}, respectively. The magnetic coupler has mutual inductance M and self-inductance L_P and L_S. Then the coupling coefficient can be derived as $k = \frac{M}{\sqrt{L_P L_S}}$. Coil losses of the IPT converter can be represented by the resistors R_p and R_s. The SS-IPT converter also contains a full-bridge rectifier composed by four diodes D_1 to D_4 at the receiver-side.

In this system, the PV panels act as a DC power source. For the wireless power transfer, the inverter converts the DC voltage into an AC voltage v_p and current i_p. The power is then picked up by the receiver coil and generates AC voltage v_s and current i_s at the receiver-side. To deliver power to the LVDC bus, the AC voltage v_s is converted back to a DC voltage by the rectifier, providing DC output voltage V_O and current I_O.

B. Operating Waveform Diagram

Fig. 3 shows the operating waveforms of the IPT converter at the transmitter-side. The switches of the inverter are turned on and off in an appropriate sequence to convert DC voltage into AC voltage. By adjusting the conduction angle α of the inverter, the fundamental component of v_p, which is v_{p1}, keeps aligned with i_p to modulate the DC input resistance. Fig. 4 shows the operating waveforms of SCC. The value of the capacitor $C_{SCC,P}$ and $C_{SCC,S}$ can be adjusted by controlling the regulation angle β. Since the operating frequencies or resonant frequencies of both sides are determined by $C_{SCC,P}$, L_P and $C_{SCC,S}$, L_S, which can be represented as $\omega_P = \frac{1}{\sqrt{L_P C_{SCC,P}}}$ and

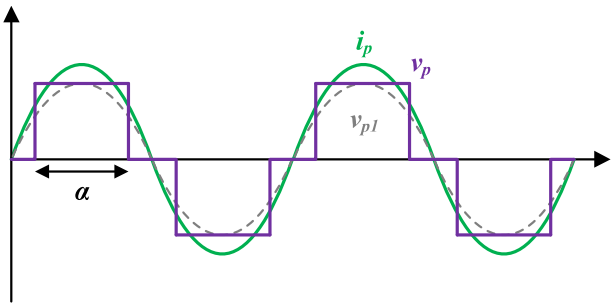

Fig. 3. Operating waveforms at transmitter-side, including AC current i_p and AC voltage v_p with its fundamental component v_{p1}.

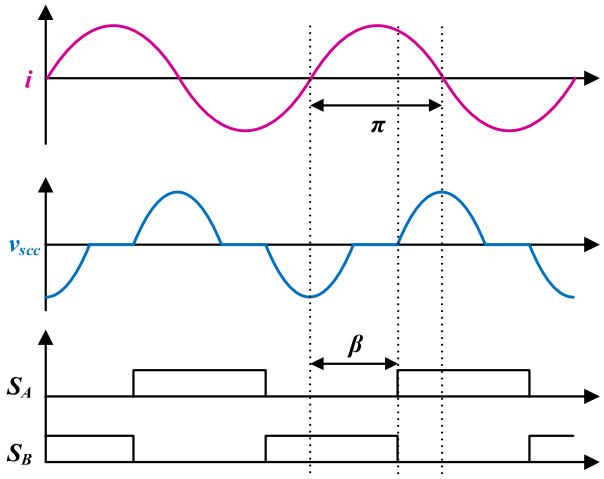

Fig. 4. Operating waveforms of SCC, including AC current at both sides $i_{s/p}$, voltage of SCC at both sides $v_{scc,s/p}$, and switch sequences S_A and S_b.

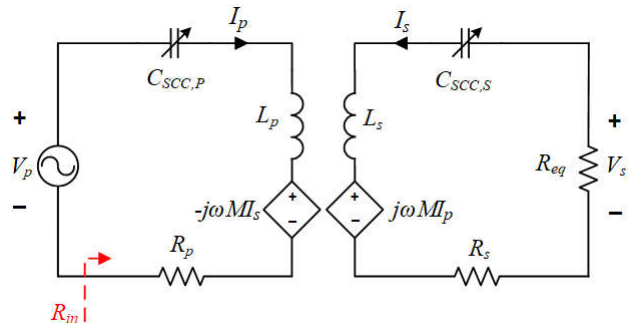

Fig. 5. Equivalent circuit model of the SS-IPT converter with SCC.

$\omega_S = \frac{1}{\sqrt{L_S C_{SCC,S}}}$, after varying operating frequency, the zero phase angle condition of IPT converter can be maintained by adjusting $C_{SCC,P}$ and $C_{SCC,S}$ at both sides.

C. Equivalent Circuit Model Analysis

The equivalent circuit model of the SS-IPT converter with SCC is derived by using fundamental harmonic approximation analysis as shown in Fig. 5. As this system operates at resonant frequency and is a circuit with high quality factor, this model is adequate for the following analysis [8]. V_P, I_P, V_S and I_S are phasors of the fundamental components of v_P, i_P, v_S and i_S, respectively. By using Kirchhoff's voltage law, the basic equations for this equivalent circuit model can be expressed as:

$$\left(R_P + jX_P\right)\boldsymbol{I}_P - jX_M\boldsymbol{I}_S = \boldsymbol{V}_p \quad (1)$$

$$-\left(R_S + R_{eq} + jX_S\right)\boldsymbol{I}_S + jX_M\boldsymbol{I}_P = 0 \quad (2)$$

where

$$X_M = \omega M \quad (3)$$

$$X_P = \omega L_P - \frac{1}{\omega C_{SCC,P}} \quad (4)$$

$$X_S = \omega L_S - \frac{1}{\omega C_{SCC,S}} \quad (5)$$

are the mutual reactance, the transmitter-side coil reactance and the receiver-side coil reactance, respectively.

The relationship between the resistive load R_{LVDC} of the LVDC bus and the equivalent output resistance R_{eq} can be expressed as:

$$R_{eq} = \frac{8}{\pi^2} R_{LVDC} \quad (6)$$

Assume that the maximum power is extracted from the PV panels and the power loss of the SS-IPT converter can be ignored (ideal case). Then the output power and the input power are identical, which can be expressed as:

$$P_{OUT} \approx P_{IN} = P_{MAX} \quad (7)$$

Then the load in maximum power condition $R_{LVDC,MAX}$ can be calculated as:

$$R_{LVDC,MAX} = \frac{V_O^2}{P_{OUT}} \approx \frac{V_O^2}{P_{MAX}} \quad (8)$$

Since the voltage of the LVDC bus can be regarded as a fixed value, for any irradiance conditions, the load in maximum power condition $R_{LVDC,MAX}$ is also a fixed value. Then from (6), the equivalent resistance R_{eq} is fixed as well, which reveals R_{eq} can represents the corresponding irradiance condition, and is denoted as $R_{eq,max}$ when MPP is achieved.

III. Analysis of Hybrid MPPT Control Strategy

The proposed hybrid control strategy achieves MPPT by regulating the DC input resistance R_{IN} to affect the output power of the PV panels. Three cases under different irradiance conditions are selected to illustrate the proposed strategy. The parameters of the simulation study are given in Table I.

A. Initial State

The system can adjust MPP by modulating operating frequency ω with capacitance compensation tracking by tuning the regulation angle β of the SCCs or the conduction angle α of the inverter at the transmitter-side. If these variables are in default, the system is in initial state. In the simulation, the initial state is at ω = 130 kHz, $\alpha = \pi$ and $\beta = 0.5\,\pi$, which makes $C_{SCC,P/S} = C_{Comp,p/s}$ and the IPT converter works with zero phase angle condition. Case (a) shown in Table II is the simulation results of the system under uniform irradiance condition without shading. It shows that the system can reach MPP at initial state under this irradiance condition.

When the irradiance condition changes, the DC input resistance R_{IN} is adjusted by the two following ways to reach the MPP again.

B. Operating Frequency Modulation with Capacitance Compensation Tracking

The relationship between the DC input resistance R_{IN} without PS modulation (i.e. when $\alpha = \pi$) and the AC input resistance R_{in} can be expressed as:

TABLE I
SIMULATION PARAMETERS

Parameter	Symbol	Value
Output voltage	V_o	60 V
Coupling coefficient	k	0.376
Coil resistance	R_P, R_S	0.26 Ω, 0.27 Ω
Self inductance	L_P, L_S	124 μH, 125 μH
Compensation Capacitance	$C_{Comp,p}$, $C_{Comp,s}$	12.0 nF, 11.9 nF
Operating frequency	$f = \omega/2\pi$	60 ~ 130 kHz
Equivalent output resistance	R_{eq}	1~60 Ω
Conduction angle	α	0.1 ~ 1 π
Regulation angle	β	0.5 ~ 0.9 π

$$R_{IN} = \frac{\pi^2 R_{in}}{8} \tag{9}$$

To analyze the AC input resistance R_{in} of the SS-IPT system, by referring Fig. 5, the dependent source $-j\omega MI_S$ at the transmitter-side is replaced by an equivalent impedance reflected from the receiver-side. Then, the AC input impedance Z_{in} can be derived as:

$$Z_{in} = Z_P + \frac{X_M^2}{Z_S + R_{eq}} \tag{10}$$

Assuming the operating frequency is set at $\omega = \omega_P = \omega_S$, the fully compensation can be achieved at both sides, both X_P and X_S are equal to zero, which reveals the input impedance of the SS-IPT converter is purely resistive. Then, the AC input resistance R_{in} can be obtained as:

$$R_{in} = R_P + \frac{X_M^2}{R_S + R_{eq}} = R_P + \frac{\omega^2 M^2}{R_S + R_{eq}} \tag{11}$$

Adjusting the operating frequency ω can theoretically change the input resistance into any desired value. However, varying the operating frequency ω of an IPT converter with fixed compensation capacitor could result in detuning issues such as low power factor. In this paper, the SCC at both sides are applied to dynamically maintain the zero phase angle condition of the IPT converter by compensating the extra inductive reactance generated by the operating frequency modulation. By controlling the regulation angle β, the equivalent capacitance of the $C_{SCC,P/S}$ can be expressed as: [9]

$$C_{SCC,P/S} = \frac{\pi C_{comp,p/s}}{2\pi - 2\beta - \sin 2\beta} \tag{12}$$

Fig. 6 shows the range of $C_{SCC,P/S}$. Since the lowest compensable range of SCC is limited by the compensation capacitor $C_{comp,p/s}$, to avoid detuning issues, the operating frequency ω can only be lower than the initial state (i.e. R_{IN} can only be lower than initial state), which is 130 kHz in the simulation. Fig. 7 gives the possible R_{IN} within the feasible operating frequency under different irradiance conditions (represented as different value of R_{eq}). In case (b), the system under non-uniform irradiance condition achieves MPP by reducing operating frequency ω to 120 kHz, R_{IN} to 26.09 Ω and setting β to 0.53 π for capacitance re-compensation.

In addition, the efficiency of this equivalent circuit model can be denoted as: [10]

$$\eta = \frac{X_M^2 R_{eq}}{X_M^2 (R_S + R_{eq}) + R_P[(R_S + R_{eq})^2 + X_S^2]} \tag{13}$$

Since X_S equals to zero in resonant condition that minimizes the value of the denominator in (13), this reveals that the capacitance compensation tracking can help to optimize the transfer efficiency.

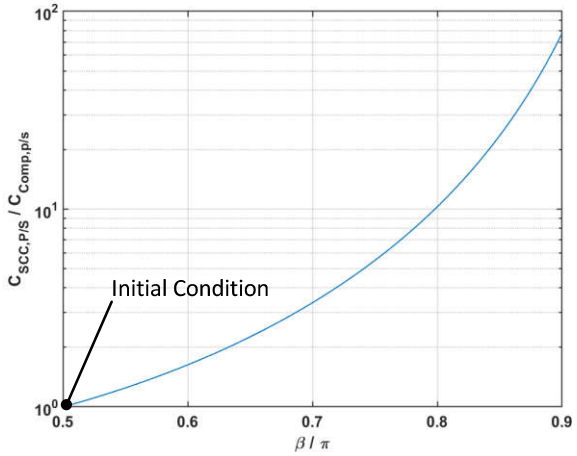

Fig. 6. Equivalent capacitance $C_{SCC,P/S}$ of the SCC versus regulation angle β. Initial condition is when $\beta = 0.5$ π, $C_{SCC,P/S} = C_{Comp,p/s}$.

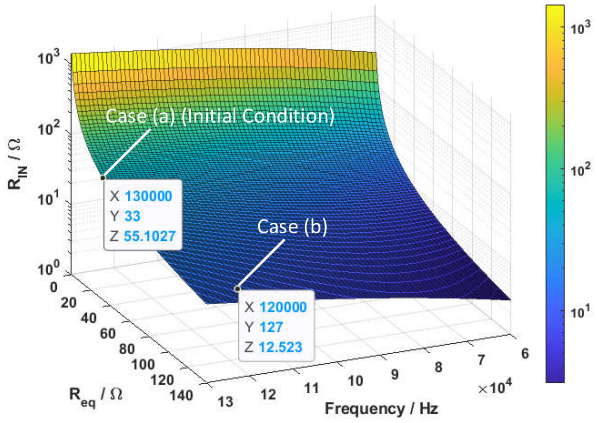

Fig. 7. DC input resistance R_{IN} versus operating frequency ω under different irradiance conditions (represented as different values of equivalent output resistance R_{eq}). Simulation results of case (a) and case (b) are highlighted.

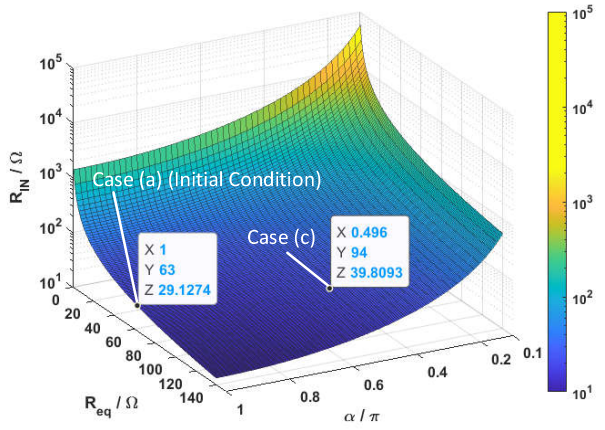

Fig. 8. DC input resistance R_{IN} versus conduction angle α under different irradiance conditions (represented as different values of equivalent output resistance R_{eq}). Simulation results of case (a) and case (c) are highlighted.

TABLE II
SIMULATION RESULTS OF THE PROPOSED SYSTEM

Case	Operating frequency, ω	Conduction angle, α	Regulation angle, β	Voltage at MPP, V_{mpp}	Maximum power, P_{MAX}	Equivalent output resistance at MPP, $R_{eq,max}$	DC input resistance at MPP, $R_{IN,MAX}$	Irradiance condition
(a)	130 kHz	π	0.5 π	56.3 V	57.6 W	63 Ω	29 Ω	Uniform w/o shading
(b)	120 kHz	π	0.53 π	27.2 V	28.4 W	127 Ω	13 Ω	Non-uniform
(c)	130 kHz	0.496 π	0.5 π	52.3 V	38.4 W	94 Ω	40 Ω	Uniform w/ shading

TABLE III
EXPERIMENT RESULTS OF THE PROPOSED SYSTEM

Case	Operating frequency, ω	Conduction angle, α	Regulation angle, β	Voltage at MPP, V_{mpp}	Maximum power, P_{MAX}	Equivalent output resistance at MPP, $R_{eq,max}$	DC input resistance at MPP, $R_{IN,MAX}$	Irradiance condition
(a)	130 kHz	π	0.5 π	56.5 V	58.3 W	57 Ω	31.8 Ω	Uniform w/o shading
(b)	120 kHz	π	0.54 π	27.8 V	29.1 W	118 Ω	13.3 Ω	Non-uniform
(c)	130 kHz	0.5 π	0.5 π	52.7 V	38.9 W	85 Ω	42.9 Ω	Uniform w/ shading

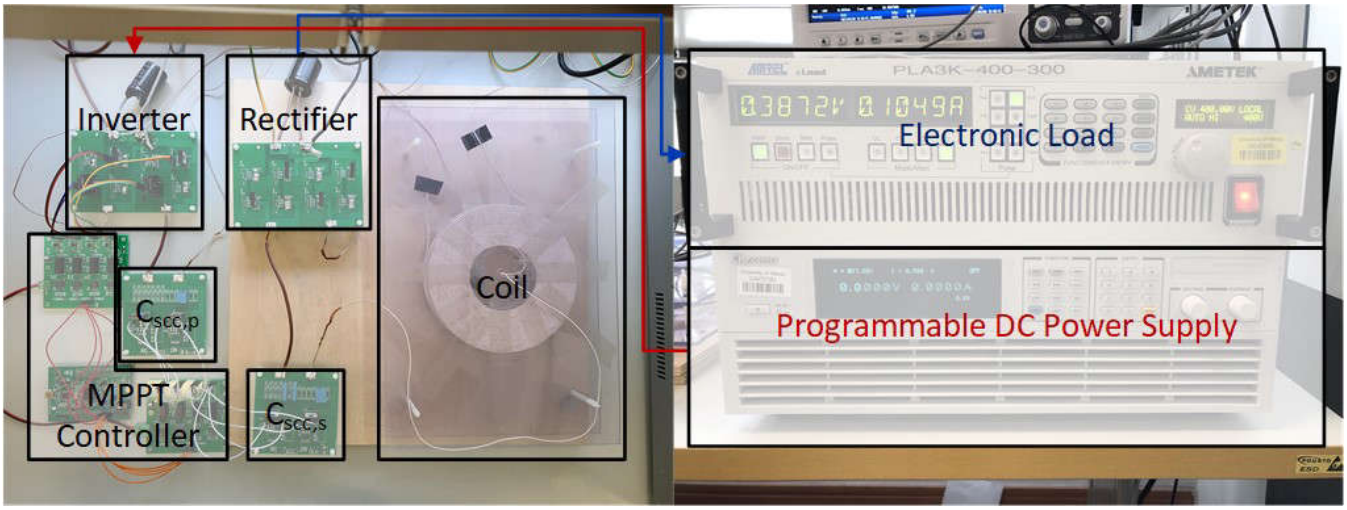

Fig. 9. Experiment platform.

C. Phase Shift Modulation

After PS modulation of the inverter, the DC input resistance R_{IN} can be denoted as: [11]

$$R_{IN}=\frac{R_{in}}{\frac{8}{\pi^2}\sin^2\frac{\alpha}{2}} \tag{14}$$

Assumed that the maximum power is extracted at the corresponding voltage V_{MPP}, then the DC input resistance at the maximum power can be derived as:

$$R_{IN,MAX}=\frac{V_{MPP}^2}{P_{MAX}} \tag{15}$$

Therefore, to obtain this DC input resistance, the conduction angle α should be set as:

$$\alpha=2\arcsin\sqrt{\frac{R_{in}}{\frac{8}{\pi^2}R_{IN,MAX}}} \tag{16}$$

Fig. 8 shows the conduction angle α versus R_{IN} under different irradiance conditions. As the conduction angle α shrinks down, the inverter can increase the value of DC input resistance. In case (c), the system under uniform irradiance condition with shading achieves MPP by adjusting the conduction angle α to 0.496 π to increase R_{IN} to 71.27 Ω.

In summary, this single-stage converter adopts hybrid MPPT control strategy that includes frequency modulation with SCC compensation and PS modulation, which can regulate the DC input resistance R_{IN} of the SS-IPT converter to track MPP under both uniform and non-uniform irradiance condition.

IV. EXPERIMENT VERIFICATION

To verify the feasibility of the IPT converter with the proposed hybrid MPPT control strategy for floating-PV system, an experiment platform in the laboratory with the same parameters as the simulation study is built for validating the simulation results, as shown in Fig. 9. A programmable DC power supply is used as PV power source and an electronic load is used to simulate the LVDC bus.

The operating waveforms of the PV-IPT system under three different irradiation conditions are shown in Fig. 10 and the corresponding MPPs of the system are shown in Fig. 11 with the experiment results summarized in Table III. In case (a), the PV-IPT system is under initial condition and reaches the MPP at 58.3 W with DC input resistance of 54.8 Ω under uniform irradiation condition without shading. In case (b), non-uniform irradiation condition is applied, and the LMPP on the left becomes GMPP. After the operating frequency ω is adjusted to 120 kHz and β is adjusted to 0.54 π, the PV-IPT system can find the MPP at 29.1 W by decreasing the input resistance to 13.3 Ω and work without detuning issue. In case (c), PV panels are under uniform irradiation condition with shading. The PV-IPT system obtains the MPP at 38.9 W after increasing the input resistance to 42.9 Ω by tuning the conduction angle from α to 0.5π.

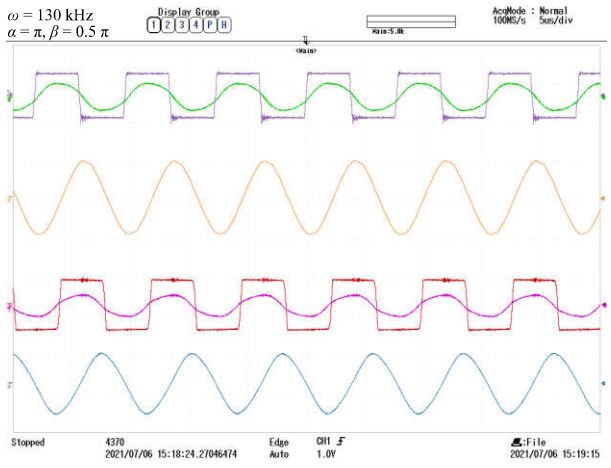

(a)

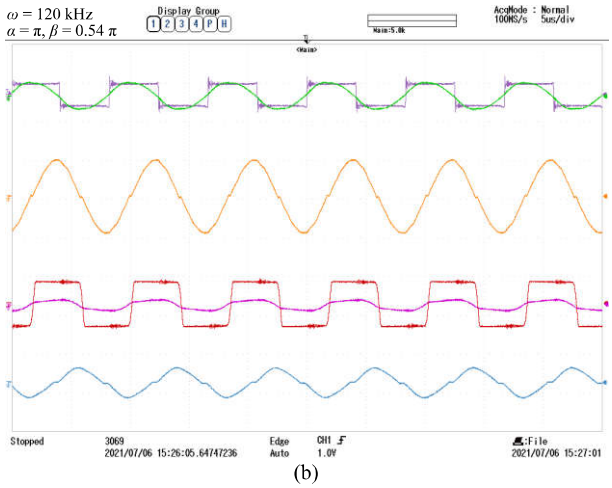

(b)

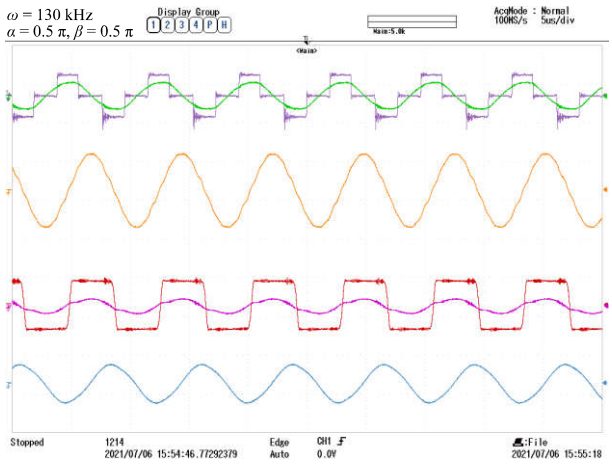

(c)

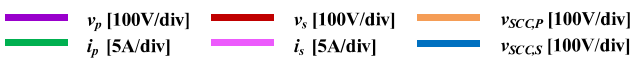

Fig. 10. Measured operating waveforms of the experiment platform when the PV panels have (a) uniform irradiance without shading, (b) non-uniform irradiance (c) uniform irradiance with shading.

V. Conclusion

An inductive power transfer system with irradiance-adaptive hybrid MPPT control strategy for floating-PV system is proposed in this paper. Wireless power transfer can help to improve the safety, reliability, and maintainability of the system. The proposed MPPT control strategy can track the maximum power point under both uniform and non-uniform irradiance condition, which is suitable for changeable weather scenarios such as lake or seashore. The hybrid MPPT control strategy is theoretically analyzed and verified with an experiment platform in the laboratory. Future work will focus on close-loop control and efficiency optimization.

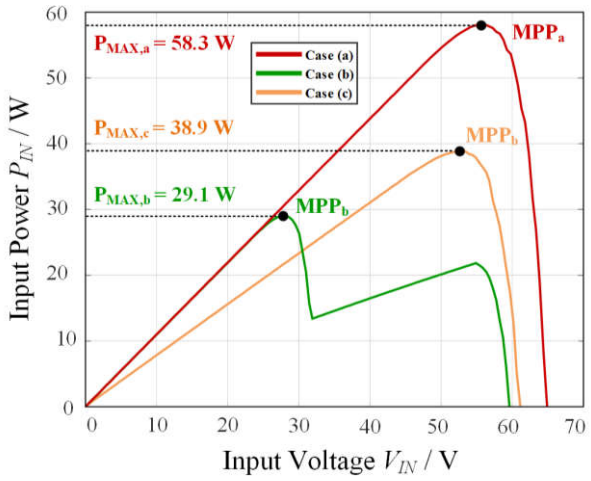

Fig. 11. Output power curves and the corresponding maximum power points in three different irradiance condition cases.

References

[1] T. Kurbatova and T. Perederii, "Global trends in renewable energy development," *in Proc. IEEE KhPI Week Advanced Tech.* , 2020, pp. 260-263.

[2] Goswami, A, Sadhu, P, Goswami, U, Sadhu, PK. *Floating solar power plant for sustainable development: A techno-economic analysis*. Environ Prog Sustainable Energy. 2019; 38:e13268. https://doi.org/10.1002/ep.13268.

[3] B. Bora et al., "Failure Mode Analysis of PV Modules in Different Climatic Conditions," *IEEE J. Photovolt.,*, vol. 11, no. 2, pp. 453-460, March 2021.

[4] Claudio Ferrara, Daniel Philipp, *Why Do PV Modules Fail?*, Energy Procedia, Volume 15, 2012, Pages 379-387, ISSN 1876-6102, https://doi.org/10.1016/j.egypro.2012.02.046.

[5] D. Singh and H. Singh, "Technical Survey and review on MPPT techniques to attain Maximum Power of Photovoltaic system," *in Proc. The 5th International Conf. Signal Proc.*, Oct. 2019, pp. 265-268.

[6] A. Ghosh, A. Ukil and A. P. Hu, "PV-Battery System with Wireless Power Transfer for LV Applications," *in Proc. The 46th Annual Conf. of the IEEE Ind. Electron. Soci.*, Oct. 2020, pp. 4283-4287.

[7] A. Ghosh, A. Ukil and A. P. Hu, "Integration of Rooftop Solar PV Generation with Wireless Power Transfer," *in Proc. IEEE PES Asia-Pacific Power Energ. Engineer. Conf*, Dec. 2019, pp. 1-5, doi: 10.1109/APPEEC45492.2019.8994668.

[8] X. Qu, H. Han, S.-C. Wong, C. K. Tse and W. Chen, "Hybrid IPT Topologies With Constant Current or Constant Voltage Output for Battery Charging Applications," *IEEE Trans. Power Electron.*, vol. 30, no. 11, pp. 6329-6337, Nov. 2015.

[9] Z. Huang, C.-S. Lam, P.-I. Mak, R. P. Martins, S.-C. Wong and C. K. Tse, "A Single-Stage Inductive-Power-Transfer Converter for Constant-Power and Maximum-Efficiency Battery Charging," *IEEE Trans. Power Electron.*, vol. 35, no. 9, pp. 8973-8984, Sept. 2020.

[10] Z. Huang, S. Wong and C. K. Tse, "An Inductive-Power-Transfer Converter With High Efficiency Throughout Battery-Charging Process," *IEEE Trans. Power Electron.*, vol. 34, no. 10, pp. 10245-10255, Oct. 2019, doi: 10.1109/TPEL.2019.2891754.

[11] Z. Huang, I.-W. Iam, I.-U. Hoi, C.-S. Lam, P.-I. Mak and R. P. Martins, "Self-Contained Solar-Powered Inductive Power Transfer System for Wireless Electric Vehicle Charging," *in Proc IEEE PES Asia-Pacific Power Energ. Engineer. Conf.*, Dec. 2019, pp. 1-6.